Universal Branch Model for the Solution of Optimal Power Flows in Hybrid AC/DC Grids

Abraham Alvarez-Bustos[a,*], Behzad Kazemtabrizi[a], Mahmoud Shahbazi[a] and Enrique Acha-Daza[b]

[a]Durham University, Department of Engineering, Lower Mountjoy, South Road, Durham, UK
[b]Tampere University, Faculty of Electrical Engineering, Korkeakoulunkatu 7 Kampusareena, 33720 Tampere, Finland

ARTICLE INFO

Keywords:
AC/DC Power Systems
Optimal Power Flows
Voltage Source Converter
Modelling
Control
AIMMS.

ABSTRACT

This paper presents a universal model formulation for solving Optimal Power Flows for hybrid AC/DC grids. The prowess of the new formulation is that it (i) provides a direct link between AC and DC parts of the grid allowing for solving the entire network within a unified frame of reference (not sequentially) and (ii) can realistically model any element within the AC/DC power grid, ranging from conventional AC transmission lines to multiple types of AC/DC interface devices such as Voltage Source Converters (VSC) by introducing additional control variables. The model is formulated in such a way that it does not make a distinction, from a mathematical perspective, between AC and DC elements and the ensuing optimal power flow (OPF) problem can be solved via model-based optimization solvers as a mathematical programming problem. Simulations carried out using a variety of non-linear gradient-based solvers in AIMMS© on a small contrived and a large realistic test system (modified PEGASE) clearly show that the universal model is on par with existing methodologies for solving OPFs both in accuracy of the solution and computational efficiency. Meanwhile, simulations carried out on a series of AC and AC/DC test systems show that the model is scalable and stays computationally tractable for larger system sizes without sacrificing convergence time.

NOMENCLATURE

Symbol	Description	Symbol	Description
y_s	Series Admittance	P_f	Active Power “from"
r_s	Series Resistance	P_t	Active Power “to"
x_s	Series Reactance	P_{loss}	VSC Losses
b_c	Shunt Susceptance	α, β, γ	VSC Losses Coefficients
N	Complex Tap Changer	f	Objective function
m_a	Tap Changer/modulation amplitude	$\mathbf{x}$	optimization Variables
k_2	Converter constant	θ_{sh}	Shift Angle
θ_{sh}	Shift Angle	$\mathbf{g}_{S_b}$	Nodal Power Balance Constraint
B_{eq}	Variable Susceptance	$\mathbf{g}_{P_f}$	Active Power Shifter Constraint
G_{sw}	PWM switch loss	$\mathbf{g}_{Q_z}$	Reactive Power Zero Constraint
Y_{br}	Branch Admittance Matrix	$\mathbf{g}_{Q_t}$	Reactive Power Q_t Constraint
v_f	Voltage “from"	$\mathbf{g}_{Pv_{dp}}$	Voltage Droop Constraint
v_t	Voltage “to"	$\mathbf{g}_{G_{sw}}$	VSC losses correction Constraint
i_f	Current “from"	$\mathbf{h}_{S_f^2}$	Loadability Constraint “from"
i_t	Current “to"	$\mathbf{h}_{S_t^2}$	Loadability Constraint “to"
S_f	Complex Power “from"	$\mathbf{L}_{S_L^2}$	Squared Power Transmission Limits
S_t	Complex Power “to"	$\mathbf{k_{dp}}$	Voltage-Power Droop Slope

* Abraham Alvarez Bustos is sponsored by Consejo Nacional de Ciencia y Tecnología (CONACyT) and Secretaría de Energía (SENER), México.
abraham.alvarez-bustos@durham.ac.uk (A. Alvarez-Bustos); behzad.kazemtabrizi@durham.ac.uk (B. Kazemtabrizi); mahmoud.shahbazi@durham.ac.uk (M. Shahbazi); enrique.achadaza@tuni.fi (E. Acha-Daza)
ORCID(s): 0000-0002-4760-4042 (A. Alvarez-Bustos)

1. Introduction

After the Paris Agreement of 2015, parties to the United Nations Framework Convention on Climate Change (UNFCCC) reached a landmark agreement to combat climate change [1, 2, 3]. To meet the targets of a fully decarbonised and sustainable electricity system by 2050, the Ten-Year Network Development Plan (TYNDP) 2020 includes approximately 80% of grid development projects related to the integration of renewable energy sources (RES) as well as the modernization of the transmission network[4]. With these projects, the European Network of Transmission System Operators for Electricity (ENTSO-E) aims to alleviate the existing problem of power flow congestion and improve the levels of operational security, as well as maximizing the operational flexibility and reliability of the Pan-European Transmission Grid. [5, 6, 7].

The idea is to create a completely controllable hybrid AC/DC power grid where the Transmission System Operators (TSO) can adjust the settings of one or multiple control devices to redirect the power flow through less congested transmission lines. This is achieved by overlaying a multi-terminal VSC-High Voltage Direct Current (HVDC) network on top of an existing AC Electric Power System (EPS) in coordination with multiple control elements, for example, Phase Shifter Transformers (PST), and Controlled Tap-Changing Transformers (CTT) within the meshed AC grid itself [8, 4, 7]. Such hybrid networks are inherently more flexible largely due to the additional control features of the VSCs [9, 10, 8].

Notwithstanding the operational benefits of hybrid AC/DC grids, these networks are more complex and therefore there is a need for proper operational planning procedures in place to ensure a continuous, safe and reliable operation of the network at all times and under all operating conditions [11, 12]. It goes without saying that any power system operational planning framework should be contingent on not only obtaining the secure operating states but also the operating states that are most economical[13]. Consequently, TSOs carry out numerous studies such as Unit Commitment, Economic Dispatch, and OPF analysis as part of the operational planning of the network [14, 15, 16, 17, 18].

The OPF problem is one of the most relevant studies from aforementioned analyses. Mathematically, in the OPF problem a chosen objective function (normally the total generation cost) is solved towards its optimum operating point subject to realistic techno-economic and security constraints of the power system [19, 13, 12]. More generally, the OPF problem is basically a constrained, non-linear, non-convex, optimization problem which for an actual EPS can contain a large number of non-linear constraints representing the physical limitations of the actual system as well as the economic boundaries within which the system needs to operate [12]. The complexity and the growth of the number of constraints is only increasing in the context of a hybrid AC/DC EPS such as the Pan-European Transmission Grid.

From an analysis perspective, the ensuing OPF problem should be computationally tractable and at the same time scalable (i.e. provide solutions to larger systems without significantly sacrificing computational time). In practice, the existing analysis tools that are able to solve OPF are mostly limited to solving AC systems with minimal capabilities to accommodate realistic network element representation and/or model libraries required for fast and accurate solutions of hybrid AC/DC networks [20, 21, 22, 23]. Moreover, any solution for a hybrid network should be able to properly reflect the intricacies of the converters' interactions and capture enough detail to be a realistic representation of the actual system. Existing solution methods normally employ a sequential method for solving the AC and DC parts of a hybrid network in sequence [24, 25, 26]. As a result, the equations per model and grid vary accordingly. Meanwhile, there are two open source non linear AC/DC OPF formulations presented in [27] and [28] to solve the AC and DC grids at the same time. The first one is an extension of the 'PowerModels.jl' package, and the second one is a Python-based framework. However, both approaches still have to model each electrical element individually. Thus, regardless of the approach taken, an extensive model library to selectively be able to incorporate various EPS elements and accommodate different network types (AC or DC) is normally needed. Furthermore, the power and voltage control of these tools are limited to the VSC variables without considering other control elements in the grid. Such limitations make it even harder to build flexibility and adaptability into the typical commercial power systems analysis tools that Transmission System Analysts (TSA) use on a daily basis.

Thus far, the closest approach to a compact model has been done by linking the traditional π branch model in series with an ideal transformer such as presented in [20]. This is very effective for the analysis of AC-only grids, however for hybrid AC/DC grids, the model is rather limited. The authors of the present paper published the first stage of generalising the MATPOWER© branch model for conventional power flow analysis of hybrid AC/DC grids in [29]. This first stage was designed exclusively for the analysis of conventional non-constrained power flows. Thus, the formulation did not include any physical constraints, neither on voltage nor power. Moreover, the first stage model cannot accurately simulate VSC losses, since they were modeled through an approximation instead of using a detailed

model. Any solutions produced with the unconstrained model for OPF will thus be undesirable for any operational planning purposes. There is also a need for a thorough testing of the model, in terms of both accuracy and computational efficiency, for both small-scale and large-scale AC/DC systems and under a variety of operating and control conditions.

This paper therefore presents a new Flexible Universal Branch Model (FUBM) for the OPF solution of hybrid AC/DC grids. It is capable of seamlessly modeling an array of network elements ranging from conventional AC and DC branches, CTT, PST, Static Compensators (STATCOM) and the VSC. Meanwhile, additional combined elements (e.g. Universal Power Flow Controller) can also be modelled using these fundamental network elements. Additionally, distinction between the AC and DC grid becomes needless thanks to the flexibility and high versatility of the model. Therefore, conventional AC OPF equations are used to solve hybrid AC/DC grids. In other words, the ensuing OPF problem formulation solves the entire network on one single frame of reference thereby eliminating the need for solving the DC and AC parts of the network in sequence. One of the main advantages of the FUBM formulation is that it is highly adaptable to any network topology with any degree of complexity and hosting a variety of control elements. To this end, the model may accommodate any control variables associated with any control elements that are active over the course of the solution by extending the vector of state variables accordingly. Similarly, the vector of constraints may be extended to accommodate any specific controls on power (e.g. scheduled power output of converters in a multi-terminal VSC-HVDC link) or on voltage (e.g. voltage control set points for an STATCOM) if deemed appropriate. As a result, the operation of a flexible and fully controllable AC/DC grid can be simulated without adding extra burden to the optimization problem or any computational effort. Thus, the FUBM for AC/DC OPF will maintain all the advantages and characteristics of the individual traditional models in a simpler, more compact, and flexible form.

The main contributions of this paper can therefore be summarised as follows: (i) The FUBM provides a direct link between AC and DC grids when modelling an AC/DC EPS allowing for solutions on a unified frame of reference, this is in essence different from existing unified models like the ones presented in [28] and [27], (ii) the FUBM provides a general framework for modelling a wide variety of AC, DC, and AC/DC elements in just one compact model to be used in operational planning problems and optimization applications in power systems, (iii) The FUBM allows the incorporation of the voltage and power control features from each one of the control elements to the optimization problem to achieve a fully flexible EPS, (iv) formulation of FUBM can be solved using a variety of optimization solvers, and as such, it is flexible enough to be incorporated in general-purpose model-based languages such as AIMMS as a mathematical programming problem.

The remainder of this paper is structured as follows: Section II introduces the FUBM in detail. It describes how does the model is able to simulate different elements of the power system and also the AC and DC grid in the same framework. It also shows the theoretical comparison between the traditional VSC model and the VSC FUBM approach. Additionally, it presents examples in how to represent complex elements by combining the internal models of the FUBM. Section III introduces various modes of control for FUBM and VSC's asserting a high degree of flexibility in the model. Section IV presents the proposed OPF problem for solving hybrid AC/DC grids modelled via FUBM, where all the optional control features are incorporated to the optimization. Finally, in Section V, case studies are presented to validate, compare and show the full performance of the FUBM formulation. Discussion of the results for small, medium and large scale test systems are also included, followed by conclusion in Section VI.

2. The AC/DC Flexible Universal Branch Model

The FUBM is an evolution of the VSC model presented in [12] after merging it with the classic π branch model in series with an ideal transformer. The proposed FUBM model is shown in Fig. 1. With this arrangement, a wide variety of elements can be simulated to represent the versatile and flexible EPS of the future, not only in AC but also in DC networks. This results in a simple but powerful universal model that interacts seamlessly with all network elements and is also capable of simulating AC/DC networks in one single frame of reference. As stated above, the benefit of this particular way of modelling would be both in versatility of the ensuing formulation in accommodating a variety of network elements both for AC and DC parts of the hybrid grid and as shall be seen later in scalability of the model. The FUBM formulation is capable of solving large-scale hybrid networks in any complexity and with a variety of different control elements to properly simulate the operation of such grids for purposes of operational planning.

The FUBM thus provides a formidable tool for both power system analysts aiming for simulating the operation of hybrid AC/DC networks as well as developers of power system analysis software packages, and the wider power systems research community, for its relative simplicity as the FUBM formulation is based on AC network equations and does not require developing separate model libraries for several network elements.

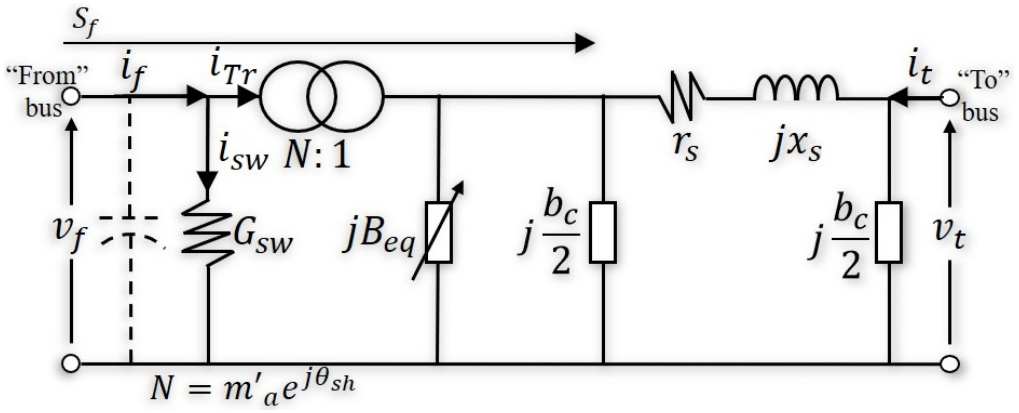

Figure 1: Flexible Hybrid AC/DC Universal Branch Model, adapted from[20]

2.1. Elements and In-Modelling

The FUBM contains one internal model (in-model) per transmission element of the EPS (one element at a time). These *in-models* share the internal components of the FUBM with each other, and therefore have distinct purposes depending on the role of the desired modeled element. As such, the FUBM is capable of modelling a series of elements ranging from standard AC transmission lines to more complex control elements such as the CTT, PST, or VSC-based elements such as the STATCOM all within one single model.

At the most basic level and with no control elements present, the AC π *Branch in-model* uses three internal components namely, the series resistance r_s, and x_s representing the series reactance and b_c representing the standard capacitive charging of the AC transmission lines. On the other hand, if a *DC Branch in-model* is required, the reactive elements of the *Branch in-model* will simply be set to a value of "zero" and the r_s will be the resistance of the DC line.

Moreover, for the *Transformer in-model*, the fixed parameters r_s and x_s represent its resistance and inductance respectively. The transformer's tap is defined by a complex tap ratio, N, which can be used to model CTT and PST as appropriate. The complex tap ratio is shown in (1). For both elements, the variable m'_a will represent the magnitude of the complex tap ratio which is meant to represent the tap changer ratio of the CTT. Similarly, if the *Transformer in-model* is meant to model a PST, θ_{sh} represents the phase shifter angle of the PST. For a conventional AC EPS with no active control elements other than the synchronous generators (i.e. no CTT or PST) only the *Branch in-model* is sufficient to model the entire EPS. However, if the AC EPS otherwise contains any control elements such as the PST and CTT, they can be incorporated by activating the m'_a and θ_{sh} as optional control variables as deemed appropriate. Using these optional control variables within the OPF formulation would also provide the means to enforce realistic operational boundaries for the PST and CTT elements in form of limits on the variables and any constraints should a power flow control be needed.

$$N = m'_a e^{j\theta_{\text{sh}}} = k_2 m_a e^{j\theta_{\text{sh}}} \tag{1}$$

The FUBM is designed to be as simple and universal as possible. Hence, it is desired that all the *in-models* share some characteristics with each other (either parameters or variables). For this reason, the usage of the traditional VSC model is not entirely suitable for this specific case. Instead, the *VSC in-model* within the FUBM is designed to be an advanced version of the VSC model presented and validated in [12, 30], where the VSC was represented by a complex tap-changing transformer and a variable shunt susceptance. In the same vein, in the FUBM *VSC in-model* the variables of the complex tap, m'_a and θ_{sh} are meant to model the amplitude modulation index and the phase shifter action of the PWM control of the actual VSC, thereby modelling the independent active and reactive power control capabilities of the actual VSC. The *VSC in-model* in the proposed FUBM approach calculates the losses of the *VSC in-model* according to the detailed model (as stated in the IEC 62751-2 standard). As a result, the *VSC in-model* of the FUBM maintains all the advantages of the traditional VSC model, while encompassing almost all of the variables and parameters that are shared between the other *in-models*. A theoretical comparison between the traditional VSC approach and the *VSC in-model* is shown in Fig.2.

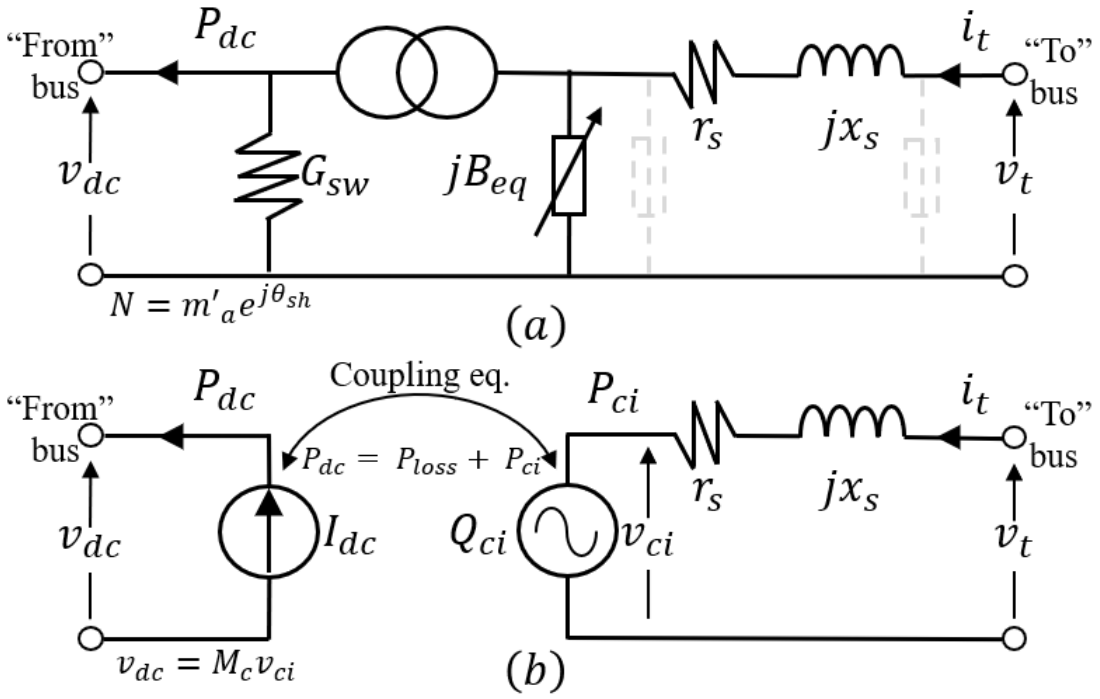

Figure 2: (a) FUBM VSC in-model, (b) Traditional VSC model

From Fig.2 it is noticeable that for both approaches, the inductive reactance jx_s and the series resistance r_s represent the magnetic interface and ohmic losses respectively. Moreover, both models present similarities in their design. Table 1 summarizes them by making a comparison between the variables and the functions of both models.

TABLE 1
FUBM VSC IN-MODEL AND TRADITIONAL MODEL COMPARISON

Function	FUBM VSC	Traditional VSC
Active Power Control	θ_{sh}	I_{dc}
AC side Reactive Control	m_a	M_c
DC side Voltage Control*b	B_{eq}	v_{dc}
Compensate AC Reactive Power*a	B_{eq}	Q_{ci}
VSC Switching losses	G_{sw}	P_{loss}
Interaction between AC and DC side	Physical link	Coupling equation

*a: Only Converters Type I [31, 18]
*b: Only Converters Type II and III [31, 18]

As seen in Table 1, control over the active power flow is a shared feature between the *VSC in-model* and the traditional VSC model. The latter defines a current source I_{dc} as a variable to control the active power flow. The *VSC in-model*, on the other hand, uses the variable θ_{sh} for this action (just like it is done by the "PST in-model").

VSCs are also well known for their AC side reactive power control capabilities. For both approaches, this is done by modifying the modulation coefficient amplitude m_a. For the *VSC in-model*, just as in the *transformers in-model*, if reactive power control is required, the *VSC in-model* has the option to set either the AC side voltage or an AC side reactive power to be meet.

One of the most desirable characteristics when using VSCs is to provide a connection of two (or more) asynchronously operating and otherwise autonomous AC grids via a common DC link. The traditional VSC model represents this by separating the grids and using controlled power sources and coupling equations to simulate an active power exchange between the AC grids through the common DC link. As seen in Fig. 2 (b), the compensation of the

reactive power of the AC side “to" bus is realised by adding a small power balance constraint in the ci node, and Q_{ci} will adjust to meet the requirements of the system. In a similar way, the FUBM *VSC in-model* compensates the reactive power by using the shunt suceptance B_{eq}. In this case, instead of adding a power balance constraint in the ci node, the reactive power flow “from" side is monitored, and Beq will be automatically adjusted within the OPF solution process to maintain zero reactive power injection to the DC link. In this paper, this reactive compensation will be called the “*Zero Constraint*".Thus, just like in the traditional approach, the FUBM simulates the isolation of the grids while maintaining the active power exchange.

Regarding to the calculation of PWM’s switching losses, the IEC 62751-2 standard recommends using a quadratic function of the VSC AC current to obtain the power losses of the converter [32]. Both the traditional and the FUBM approach follow this recommendation. For the traditional model, P_{loss} is the variable that is adjusted in function of the current; whereas for the *VSC in-model* the variable G_{sw} correspond to the actual VSC losses, thus the power loss in both cases must be the same. Since theoretically there is no upper limit on how much switching losses a VSC can have, both the P_{loss} and the G_{sw} variables are normally set with a lower bound of zero and unbounded above. Equations (4) and (5) show the calculation of the power loss for both approaches.

$$P_{loss}^{Trad} = P_{loss}^{\text{FUBM}} \tag{2}$$

$$P_{loss}^{\text{FUBM}} = v_f i_{sw} = v_f^2 G_{sw} \tag{3}$$

$$-P_{loss}^{Trad} + \gamma i_t^2 + \beta i_t + \alpha = 0 \tag{4}$$

$$-v_f^2 G_{sw} + \gamma i_t^2 + \beta i_t + \alpha = 0 \tag{5}$$

As can be seen from both, the power loss equations above, and the Fig 2, the interaction between the AC side and the DC side is carried out by either a coupling equation, for the traditional approach, or through a physical link for the *VSC in-model*. Regardless of the design of both approaches, mathematically they represent the same equation. From the perspective of the FUBM, this equation is obtained as a result of power injections in node “from". Where the active power from the AC network minus the converter losses will be the active power of the DC network, which matches the coupling equation used by the traditional model. This equation is expressed in (6).

$$P_{dc} = P_{ci} - P_{loss} \tag{6}$$

There are mainly three operational limits for any VSC. Figure 3 shows each one of them, which represent the constraints that both the Traditional VSC approach and the FUBM have to meet.

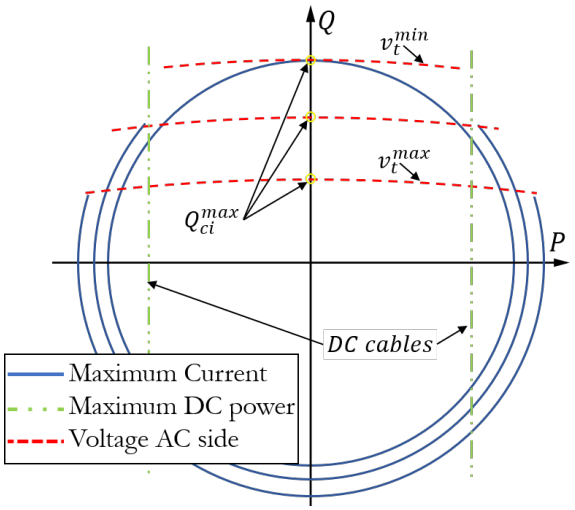

Figure 3: VSC Operational Limits, Modified from [33]

The first constraint is the maximum current through the switching devices (i.e. IGBTs). It can be appreciated in Fig 3 as an MVA circle in the power plane where maximum current and actual AC voltage are multiplied. If the AC voltage decreases so will also the MVA capability [33]. The constraint is expressed mathematically in (7).

$$P_t^2 + Q_t^2 \leq \left(v_t i_t^{max}\right)^2 \tag{7}$$

The second constraint is the reactive power compensation limit Q_{ci} which is mainly dependent on the voltage difference between the AC and the DC voltage. From Figure 3, it is noticeable that the maximum reactive power is not a fixed value, therefore the limit for it is expressed as a constraint in (8) for the traditional model, and in (9) for the VSC *in-model* [33][34]. Both equations show that Q_{ci}^{max} and B_{eq}^{max} represent the same maximum reactive power operational limit. Additionally in Fig. 3, is clear that the reactive power lower limit is automatically constrained by (7).

$$Q_{ci}^{max} = \frac{v_{ci}|v_t| - |v_t|^2}{x_s} \quad \text{Where:} \quad v_{ci} = \frac{v_{dc}}{k_2 M_c} \tag{8}$$

$$Q_{B_{eq}}^{max} = v_{ci}^2 B_{eq}^{max} = \frac{v_{ci}|v_t| - |v_t|^2}{x_s} \tag{9}$$

$$B_{eq}^{max} = \frac{v_{ci}|v_t| - |v_t|^2}{v_{ci}^2 x_s} \quad \text{Where:} \quad v_{ci} = \frac{v_{dc}}{k_2 m_a} \tag{10}$$

The third constraint is the maximum DC current through the DC cable. If the rate of the cable is smaller than the rate of the VSC it may limit the maximum active power transfer to the DC grid. This constraint is automatically added to the optimization problem by adding the thermal limits of the DC lines.

After the theoretical comparison between the VSC Traditional model and the *VSC in-model* of the FUBM it is clear that both approaches keep the same amount of variables and constraints and as a result, no additional burden is necessary for the simulations.

The FUBM is also capable of modelling STATCOMs explicitly. Unlike other simpler approaches which model the STATCOM as a controllable voltage source, the *STATCOMs in-model* is a more accurate representation of the device. This is achieved by making use of the *VSC in-model* with a fixed DC voltage as shown in Fig. 4. This STATCOM model was presented separately in an earlier publication [35] and is now brought together within the FUBM for the sake of completeness.

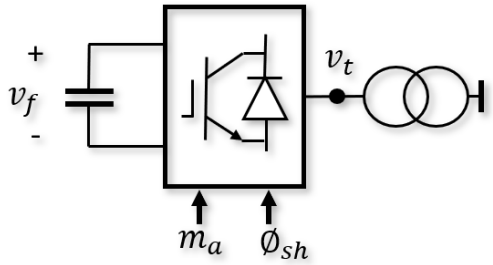

Figure 4: STATCOM-inmodel schematic representation using VSC

In this section, the theoretical underpinnings of all the *in-models* within the FUBM have been described. The selection of a specific *in-model*, and whether any of them are used to exert any control actions within the EPS, is done automatically by activating the appropriate state and control variables (i.e. the *in-model* settings) pertaining to the specific in-models as shown in Table 2. Notice that the k_2 parameter will depend on the type of the VSC to model - this variable can be used to accommodate any VSC type from normal two-level converters to modular multi-level converters if needs be. For a two-level VSC, the k_2 value will be $\sqrt{3}/2$.

TABLE 2
SETTINGS FOR THE DESIRED IN-MODEL

Parameter or Variable	Branch DC	Branch AC	CTT	PST	VSC	STATCOM
G_{sw}	0	0	0	0	$*^b$	$*^b$
B_{eq}	0	0	0	0	$*^b$	$*^b$
θ_{sh}	0	0	0	$*^b$	$*^b$	$*^b$
k_2	1	1	1	1	$*^a$	$*^a$
m_a	1	1	$*^b$	1	$*^b$	$*^b$
b_c	0	$*^a$	0	0	0	0
r_s	$*^a$	$*^a$	$*^a$	$*^a$	$*^a$	$*^a$
x_s	0	$*^a$	$*^a$	$*^a$	$*^a$	$*^a$
v_f	free	free	free	free	free	fixed

$*^a$: *in-model* parameter $*^b$: *in-model* active optimization variable

2.1.1. Combined in-models

Additional various elements in the EPS can be modelled using different combinations of the described *in-models*. For example, the Unified Power Flow Controller (UPFC) from [36], can be easily modelled by setting two *VSC in-models* in a back to back configuration with a branch in parallel as shown in figure 5. Controls in each one of the *in-models* can be individually adjusted to accurately simulate the controllable reactive and active power of the UPFC as needed [37]. This approach will also simulate the switching losses of the VSCs. Table 3 presents the settings each one of the in-models to accurately simulate the UPFC.

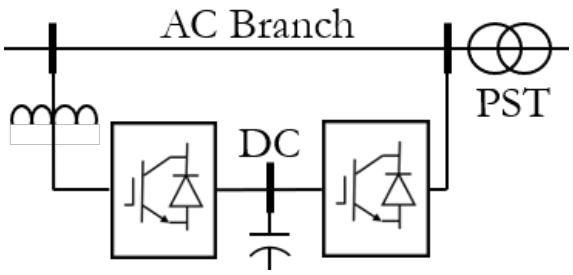

Figure 5: UPFC schematic representation using *in-models*

Since the FUBM does not create a distinction between the AC and the DC grid, combinations inside the DC grid could also be created. For example, the Bidirectional DC Converter from [38], could be represented as shown in Fig. 6. Where two *VSC in-models* are set in a back to back configuration, and each one of them is connected to a Low and High Voltage DC circuit. The controls over the B_{eq} and θ_{sh} are deactivated as shown in Table 3. Only both m_a are used for voltage control in both sides. This configuration allows to accurately represent the switching losses inside the Bidirectional DC converter using the G_{sw} variable of both VSC *in-models*.

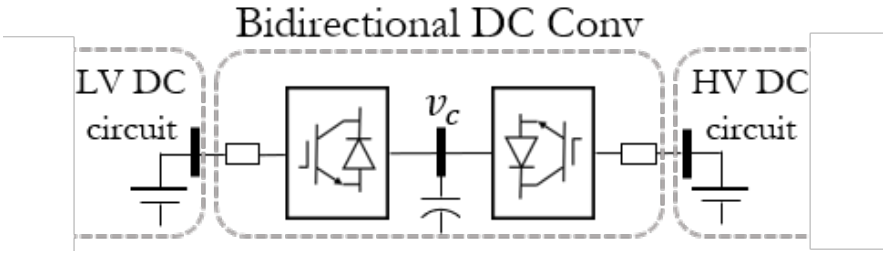

Figure 6: Bidirectional DC Converter schematic representation using *in-models*

TABLE 3
COMBINED IN-MODELS SETTINGS

Parameter	UPFC				Bidirectional DC Conv	
or Variable	AC branch	VSC 1	VSC 2	PST	VSC 1	VSC2
G_{sw}	0	$*^b$	$*^b$	0	$*^b$	$*^b$
B_{eq}	0	$*^b$	$*^b$	0	0	0
θ_{sh}	0	$*^b$	$*^b$	$*^b$	0	0
k_2	1	$*^a$	$*^a$	$*^a$	$*^a$	$*^a$
m_a	1	$*^b$	$*^b$	$*^b$	$*^b$	$*^b$
b_c	0	0	0	0	0	0
r_s	$*^a$	$*^a$	$*^a$	$*^a$	$*^a$	$*^a$
x_s	$*^a$	$*^a$	$*^a$	$*^a$	$*^a$	$*^a$
v_f	free	free	free	free	free	free

$*^a$: in-model parameter, $*^b$: in-model optimization variable

2.2. FUBM Equations

In this paper, the power balance equations and injections for the FUBM approach are expressed following Matpower's convention which can be found in [20]. However it is worth to highlight that the equations presented in this paper are explicitly defined for the FUBM as a new model following this convention.

By applying Kirchhoff's Law to the FUBM model in Fig. 1, the $[2 \times 2]$ model's admittance matrix Y_{br} can be obtained. This is shown in (11), (12) and (13). Notice that the sub index f and t in (12), represent the connection bus "from" and "to" respectively; e.g. y_{ff} will contain the sum of all the admittance elements connected to "from" bus. Also observe that for the *VSC in-model*, the v_f represents the DC voltage side v_{dc} and hence, the v_t represents the AC voltage side v_{ac}.

$$\begin{bmatrix} I_{br} \end{bmatrix} = \begin{bmatrix} Y_{br} \end{bmatrix} \begin{bmatrix} V_{br} \end{bmatrix} \tag{11}$$

$$\begin{bmatrix} i_f \\ i_t \end{bmatrix} = \begin{bmatrix} y_{ff} & y_{ft} \\ y_{tf} & y_{tt} \end{bmatrix} \begin{bmatrix} v_f \\ v_t \end{bmatrix} = \begin{bmatrix} Y_{br} \end{bmatrix} \begin{bmatrix} v_f \\ v_t \end{bmatrix} \tag{12}$$

$$Y_{br} = \begin{bmatrix} G_{sw} + (y_s + j\frac{b_c}{2} + jB_{eq})\frac{1}{m_a'^2} & \frac{-y_s}{m_a' e^{-j\theta_{\text{sh}}}} \\ \frac{-y_s}{m_a' e^{j\theta_{\text{sh}}}} & y_s + j\frac{b_c}{2} \end{bmatrix} \tag{13}$$

Complex branch power flow "from" side and "to" side of the FUBM is given by (15).

$$S_{br} = V_{br} I_{br}^* \tag{14}$$

$$\begin{aligned} S_f &= [v_f][i_f^*] = [v_f][y_{ff} v_f + y_{ft} v_t]^* \\ S_t &= [v_t][i_t^*] = [v_t][y_{ft} v_f + y_{tt} v_t]^* \end{aligned} \tag{15}$$

$$\tag{16}$$

The calculation of the Power Injections for an EPS with n_l lines and n_b buses can be expressed in matrix form by multiplying both branch admittance matrices "from" side $\mathbf{Y_f}$ and "to" side $\mathbf{Y_t}$ times their respective vector of Voltages $\mathbf{V_f}$ and $\mathbf{V_t}$ as seen in (17). These last ones are calculated by multiplying the branch connection matrices $\mathbf{C_f}$ and $\mathbf{C_t}$ times the vector of nodal voltages $\mathbf{V}$. Each connection matrix has a size of $[n_l \times n_b]$, and contains an indicator with the value of 1 where the branch element "from" or "to" side connects with the bus. All the non nodal incidences of C_f and C_t are zero. [20].

$$\begin{aligned} \mathbf{S_f} &= \mathbf{V_f}[\mathbf{Y_f V}]^* = \mathbf{C_f}[\mathbf{V}][\mathbf{Y_f V}]^* \\ \mathbf{S_t} &= \mathbf{V_t}[\mathbf{Y_t V}]^* = \mathbf{C_t}[\mathbf{V}][\mathbf{Y_t V}]^* \end{aligned} \tag{17}$$

$$\begin{aligned} \text{Where,} \quad & \mathbf{Y_f} = [\mathbf{Y_{ff}}]\mathbf{C_f} + [\mathbf{Y_{ft}}]\mathbf{C_t} \\ \text{And,} \quad & \mathbf{Y_t} = [\mathbf{Y_{tf}}]\mathbf{C_f} + [\mathbf{Y_{tt}}]\mathbf{C_t} \end{aligned} \tag{18}$$

From (17) the active and reactive power injections can be calculated as:

$$\begin{aligned}\mathbf{P_f} &= Real\big(\mathbf{S_f}\big) = Real\big(\mathbf{C_f}[\mathbf{V}][\mathbf{Y_f}\mathbf{V}]^*\big)\\ \mathbf{P_t} &= Real\big(\mathbf{S_t}\big) = Real\big(\mathbf{C_t}[\mathbf{V}][\mathbf{Y_t}\mathbf{V}]^*\big)\\ \mathbf{Q_f} &= Imag\big(\mathbf{S_f}\big) = Imag\big(\mathbf{C_f}[\mathbf{V}][\mathbf{Y_f}\mathbf{V}]^*\big)\\ \mathbf{Q_t} &= Imag\big(\mathbf{S_t}\big) = Imag\big(\mathbf{C_t}[\mathbf{V}][\mathbf{Y_t}\mathbf{V}]^*\big)\end{aligned} \tag{19}$$

2.3. Modelling Hybrid AC/DC EPS using FUBM

The most fundamental AC/DC grid is the VSC-HVDC Transmission Link point-to-point (PTP) configuration. It is shown schematically in Fig. 7(a). When incorporating this widely used configuration in conventional power flow formulations (as well as OPF formulations) using the Traditional VSC model, a separation between the AC and DC Grids becomes evident. The split is illustrated in Fig. 7(b). As a result, three sets of system equations have to be solved individually in order to find a solution for the whole AC/DC Grid, one for the AC side, one for the DC side and one for the interface between them (as the set of coupling equations representing the active power exchange between the AC and the DC grid for all VSCs). Steady State analyses of AC grids are solved using vectors since the voltages are expressed as complex numbers. Furthermore, AC voltage angles are calculated with regards to one reference bus angle per isolated grid. DC grids on the other hand are analysed using scalars since only the voltage magnitude is relevant for their calculations. It follows that from a purely mathematical perspective, when modelling a hybrid AC/DC EPS using the traditional approach, the AC and DC counterparts are essentially modelled distinctly and also interfaced using the set of coupling equations to be able to simulate the power exchange in the HVDC link.

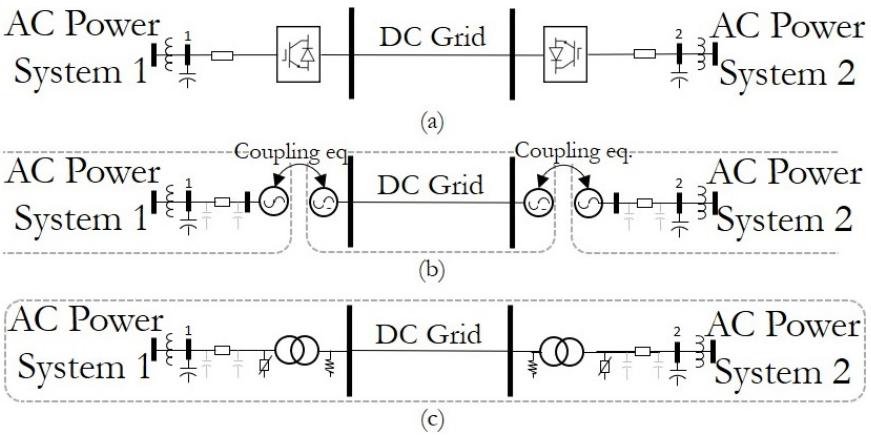

Figure 7: (a) Classic VSC-HVDC link, (b) Traditional Separated grids generator Link, (c) Unified Hybrid Grids Link with FUBM

Alternatively, as shown in Fig. 7(c), the whole hybrid AC/DC grid can be solved on one single frame of reference when modelled using the FUBM approach. As explained in Section 2.1, the *VSC in-model* compensates the reactive power of the AC side while seamlessly keeping the physical link between the AC and DC side. As a result, in an HVDC PTP configuration, the reactive power compensation only needs to be satisfied in one of the two VSCs terminals since the remaining one will be naturally compensating it thanks to the physical connection. Thus, by taking advantage of the reactive power compensation from the *Zero Constraint*, only active power is exchanged though the DC link. For this reason, there is no need for any additional coupling equations to maintain power balance in the DC link, thereby removing the need for making any distinction between AC and DC counterparts nor for solving the AC and DC parts sequentially. Table 4 compares the number of equations for a PTP configuration for both approaches.

It follows from above that since FUBM models everything in one single frame of reference both AC and DC variables are mathematically represented as complex phasors. Thus, essentially the scalar DC voltage magnitude can be represented as a complex phasor with “zero" imaginary part, or in other words with a voltage phase angle of “Zero". In this unified approach, just as in an any AC system, one reference bus phase angle is needed per isolated grid relative to which all the other nodal phase angles are calculated. Since the Voltages in the AC side do have an imaginary part, and do not in the DC side, it is recommended to use a DC node as reference. Nevertheless, it should be noted that the reference angle, as the name implies, is only a reference. What really matters is the angular difference between the AC

TABLE 4
PTP HVDC EQUATION COMPARISON

Description of the Equation	Number of Equations Traditional	FUBM
Active Power Control	1	1
DC side Voltage Control	1	1
Compensate AC Reactive Power	2	1
VSC Switching losses	2	2
Interaction between AC and DC side	2	2*
Total Number of Equations	8	5

** Non explicit, Physical Link inside the FUBM*

nodes that are interconnected with each other, because this angular difference will have an impact over the AC power flow. If the interconnected nodes have the same voltage angle or a voltage angle of zero, like in the DC side, it means that the DC power flow is purely dictated by the voltage magnitude. Consequently, if the reference angle is chosen in the AC side, it is possible that the DC voltage angles do have a non zero constant angle which is maintained trough the entire DC grid (hence preserving the DC side characteristics). Mathematically, the FUBM can be treated as a normal AC element, and accordingly AC OPF equations can be used to solve the hybrid AC/DC power grid. As a result, some coding time and effort can be saved.

3. VSC Control Modes

Depending on the operational and control requirements of the hybrid EPS, the VSCs can be set to control the voltage, active and reactive power or all or a combination of both power and voltage control. This section presents different control settings/modes for the VSC that are commonly used in the industry and how the these control actions are mathematically incorporated in the FUBM. In practice, VSCs have seven different control modes depending on their role in the hybrid EPS, they can be seen in Table 5 [31, 39].

TABLE 5
VSC CONTROL MODES

Control Mode	Constraint 1	Constraint 2	VSC Control Type
1	θ_{sh}	v_{ac}	I
2	P_f	Q_{ac}	
3	P_f	v_{ac}	
4	v_{dc}	Q_{ac}	II
5	v_{dc}	v_{ac}	
6	v_{dc} droop	Q_{ac}	III
7	v_{dc} droop	v_{ac}	

The VSCs are divided to three types and each one has a specific set of control modes. Moreover, there are two active control constraints per VSC control mode. Each constraint combination maintains either a constant power, a constant voltage, voltage droop characteristic or a combination of them. Each individual control constraint has a direct impact over the system feasible region. Consequently, a set of rules have to be followed to avoid operational and resolvability problems when implementing Multi-terminal DC (MTDC) grids or HVDC-Links. In the interest of keeping the voltage of the DC grid within certain limits, there must be at least one VSC type #II or type #III for voltage regulation. If the VSC type #II is selected, there should not be more than one of them in each DC network, and all remaining converters in it must be type #I. Similarly, in an MTDC grid where n VSCs type #III are set, the remaining m VSCs must be type #I. Additionally, all VSC type #III require the addition of the voltage droop characteristic to the formulation. This control characteristic will depend on the application to be used for. Figure 8 shows a couple of examples where a linear Power-Voltage control, a non-linear Power-Voltage control, and a linear Current-Voltage control are presented. Finally, when connecting wind farms, photovoltaic power plants, energy storage devices or passive networks via VSC, type #I converter must be used[31, 40]. Regardless of what type of VSC model is being used (either the traditional or the FUBM approach), both must follow the described rules.

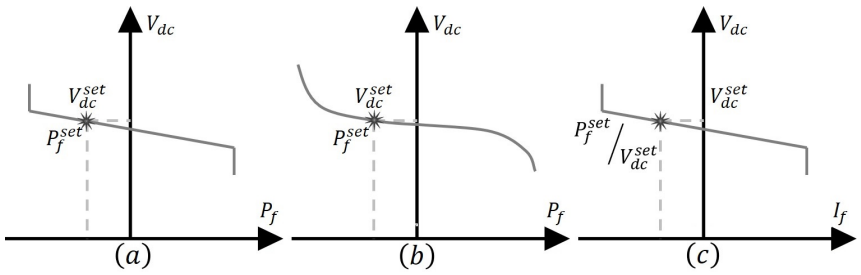

Figure 8: (a) $v_{dc} - P_f$ droop. (b) Adaptive droop. (c) $v_{dc} - i_f$ droop

As it was described in Section 2.1, Both VSC approaches (traditional and FUBM) should compensate the AC side reactive power of the grid. For an MTDC link with h VSC terminals, using the traditional modelling approach, all VSC models must do this compensation for all VSC terminals. On the other hand, using FUBM *VSC in-model* the *zero constraint* should only be met for $h - 1$ VSC terminals. It follows that there will be no reactive power in the DC side of the remianing VSC terminal without the need for activating the *zero constraint* for that terminal. This mathematical advantage over the traditional VSC modelling approach is possible thanks to the unique physical link that the FUBM provides between the AC and the DC sides of the EPS.

The FUBM uses the converter types as identifiers to easily use this advantage. Thus, for MTDC links where one converter type #II has been selected for voltage regulation, only the remaining converters type #I will use the suceptance B_{eq} to compensate the reactive power and thus meet the *zero constraint*. Similarly, for MTDC links with n VSC type #III and m type #I, all m VSC type #I have to meet the *zero constraint*, but only $n - 1$ VSC type #III have to meet this constraint. Again the last one will be automatically compensated without the need of any activation. Table 6 summarizes the voltage regulation structure.

TABLE 6
VSCs STRUCTURE ON A MTDC GRID

MTDC Voltage Regulation Type	Max Number of VSC for Voltage Regulation	Min number of VSC for Zero Contraint	Max number of VSC in the MTDC Grid
Constant Voltage	1 VSC type #II	m VSC type #I	m+1
Voltage Droop Control	n VSC type #III	m VSC type #I and n-1 VSC type #III	m+n

Regarding the control modes, the FUBM is designed to incorporate each one of the aforementioned VSC control constraints individually as it is described in Section 2.1. As a result, the *VSC in-model* is not restricted by the pair of control constraints of each VSC control mode of Table 5. Therefore, it has the option to activate or deactivate the desired control over the modelled element depending on the operational requirements of the EPS.

4. Flexible OPF Formulation using FUBM

This section presents the OPF formulation for the solution of hybrid AC/DC EPS when modelled using the FUBM. The presented formulation is the most complete one since it includes the optional power and voltage controls that were described in Sections 2 and 3. It should be noted that these optional controls can be activated or deactivated as needed. Therefore the formulation using FUBM can be used to solve OPF for AC, DC or hybrid AC/DC networks.

The OPF objective function f can vary depending on the aim of the study. For this paper the aim is to minimise the total generation cost as this is a common aim in the industry. Therefore, f is the summation of the of individual polynomial cost functions (typically quadratic) for each generator as shown in (20).

$$f(\mathbf{x}) = \sum_{i=1}^{ng} f_P^{\{i\}}(P_g^{\{i\}}) + f_Q^{\{i\}}(Q_g^{\{i\}}) \tag{20}$$

The Hybrid AC/DC OPF problem using FUBM can be compactly formulated in equations (21) to (28).

$$\min_{\mathbf{x}} \quad f(\mathbf{x}) \tag{21}$$

subject to:

$$\mathbf{g}_{S_b}(\mathbf{x}) = \mathbf{0} \tag{22}$$
$$\mathbf{g}_{P_f}(\mathbf{x}) = \mathbf{0} \tag{23}$$
$$\mathbf{g}_{Q_z}(\mathbf{x}) = \mathbf{0} \tag{24}$$
$$\mathbf{g}_{Q_t}(\mathbf{x}) = \mathbf{0} \tag{25}$$
$$\mathbf{g}_{Pv_{dp}}(\mathbf{x}) = \mathbf{0} \tag{26}$$
$$\mathbf{g}_{G_{sw}}(\mathbf{x}) = \mathbf{0} \tag{27}$$
$$\begin{aligned} \mathbf{h}_{{S_f}^2}(\mathbf{x}) &\leq \mathbf{L}_{{S_L}^2} \\ \mathbf{h}_{{S_t}^2}(\mathbf{x}) &\leq \mathbf{L}_{{S_L}^2} \end{aligned} \tag{28}$$

where:

$$\mathbf{x} = [\mathbf{P_g}, \mathbf{Q_g}, \mathbf{V_a}, \mathbf{V_m}, \mathbf{B_{eq}}, \theta_{\mathbf{sh}}, \mathbf{m_a}, \mathbf{G_{sw}}]^\intercal \tag{29}$$
$$\mathbf{x}_{min} \leq \mathbf{x} \leq \mathbf{x}_{max} \tag{30}$$

Equality constraints in (22) are the classical non-linear real and reactive power balance equations for all AC and DC nodes indistinctly. It is noted that for the DC grid, the reactive power balance results in a value of zero since the reactive injections to the DC grid are controlled by the variable B_{eq} in conjunction with the *"Zero Constraint"* given in (24). Thus, for a specified number of generation units to satisfy a particular pattern of load per bus, the complex power balance equations of the system using FUBM are given by (31) [20].

$$\mathbf{g}_{S_b}(\mathbf{x}) = \mathbf{S_{bus}}(\mathbf{x}) + \mathbf{S_d} - \mathbf{S_g} = \mathbf{0} \tag{31}$$
$$\text{Where,} \qquad \mathbf{S_{bus}}(\mathbf{X}) = [\mathbf{V}]{\mathbf{I_{bus}}}^* = [\mathbf{V}]{\mathbf{Y_{bus}}}^*\mathbf{V}^* \tag{32}$$

As it can be observed, for the calculation of the power balance constraints, it is necessary to obtain the admittance matrix $\mathbf{Y_{bus}}$. It is worth highlighting that without FUBM, the construction of $\mathbf{Y_{bus}}$ will have to be done considering different equations for each element model. Moreover, for modelling hybrid AC/DC grids, as shown previously, the power balance constraints will be split in a set of equations for each isolated grid which are then needed to be coupled using the DC power balance coupling equations as shown in Section 2.3.

The optional control constraints (23) to (27) are modelled in order to capture maximum operational flexibility for the EPS. Further description of each optional control constraint within the FUBM is included below. Additionally, the sets $\mathcal{I}_{sh}$, $\mathcal{I}_{cct}$, $\mathcal{I}_{vsc}$ contain all the PSTs, CCTs, and VSCs respectively.

For active power control, the required value for all *PST* and *VSC in-models* can be set in the vector $\mathbf{P_f^{set}}$. The full active power control constraint of (23) is shown in (33).

$$\mathbf{g}_{P_f}^{\{i\}}(\mathbf{x}) = Real\left({\mathbf{S_f}}^{\{i\}}(x)\right) - {\mathbf{P_f^{set}}}^{\{i\}} \quad \forall i \in \mathcal{I}_{sh} \text{ or } \mathcal{I}_{vsc} \tag{33}$$

Regarding to reactive power control of the “to" side of CTTs or AC side for VSCs, control constraint in (34) is set to meet the reactive power reference value $\mathbf{Q_t^{set}}$.

$$\mathbf{g}_{Q_t}^{\{i\}}(\mathbf{x}) = Imag\left({\mathbf{S_t}}^{\{i\}}(x)\right) - {\mathbf{Q_t^{set}}}^{\{i\}} \quad \forall i \in \mathcal{I}_{vsc} \tag{34}$$

As explained in Section 2.1, the reactive power compensation in the *VSC in-model* is represented by the *"Zero constraint"*. It can be seen in (24) and (35). This control ensures that there is no reactive power flow in the DC network.

$$\mathbf{g}_{Q_z}^{\{i\}}(\mathbf{x}) = Imag\left(\mathbf{S_f}^{\{i\}}(x)\right) - \mathbf{zero} \quad \forall i \in \mathcal{I}_{vscI} \tag{35}$$

When VSC Voltage droop control is implemented, the power injected to the DC grid will be a function of the VSC DC voltage. Furthermore, the droop equation will vary depending on the control type as shown in Fig. 8. Even though Voltage Droop control strategy with a specified ramp or function is more commonly addressed in Power Flow studies [17, 41], in operational day-ahead planning the settings of the Droop Control ramps do not change on a daily basis. Instead, they have been pre-set based on the capability characteristics of each VSC station and the medium/long term operational conditions of the system[42]. Therefore, these pre-set ramps have to be considered for the short term or day-ahead optimisation. As a result, they been added as part of the FUBM OPF formulation, which can be activated or deactivated depending on the requirements and aims of the analysis. Equation (36) presents the traditional voltage-power $v_{dc} - P_f$ standard droop control equation. The parameter k_{dp} represents the slope for the $v_{dc} - P_f$ control.

$$\mathbf{g}_{Pv_{dp}}^{\{i\}}(\mathbf{x}) = -Real\left(\mathbf{S_f}^{\{i\}}(x)\right) + \mathbf{P_f^{set}}^{\{i\}} - k_{dp}\left(\mathbf{v_f^{\{i\}}} - \mathbf{v_f^{set}}^{\{i\}\,set}\right) \quad \forall i \in \mathcal{I}_{vscIII} \tag{36}$$

VSC in-model losses are calculated as specified in the standard IEC 62751-2 [32]. The VSC power loss constraint is shown in (37).

$$\mathbf{g}_{G_{sw}}^{\{i\}}(\mathbf{x}) = -\mathbf{v_f^2}^{\{i\}}\mathbf{G_{sw}}^{\{i\}} + \gamma\mathbf{i_t^2}^{\{i\}} + \beta\mathbf{i_t}^{\{i\}} + \alpha \quad \forall i \in \mathcal{I}_{vsc} \tag{37}$$

The limits on the transmission lines (branch limits) for all *in-models* are represented as inequality constraints as shown in (28), and expanded in (38) as one set of matrix equations. Notice that these equations also include the PQ-capability limit for all VSCs.

$$\begin{aligned}\left(\mathbf{P_f}^{\{i\}}(x)\right)^2 + \left(\mathbf{Q_f}^{\{i\}}(x)\right)^2 &\leq \left(\mathbf{L}_{S_L}^{\{i\}}\right)^2 \quad \forall i \in \mathcal{I}_{\text{FUBM}} \\ \left(\mathbf{P_t}^{\{i\}}(x)\right)^2 + \left(\mathbf{Q_t}^{\{i\}}(x)\right)^2 &\leq \left(\mathbf{L}_{S_L}^{\{i\}}\right)^2 \quad \forall i \in \mathcal{I}_{\text{FUBM}}\end{aligned} \tag{38}$$

Finally the upper and lower limits for the vector of state variables $\mathbf{x}$, are set in the vectors $\mathbf{x}_{max}$ and $\mathbf{x}_{min}$ respectively. It is worth mentioning that when using the optional voltage control for either CTTs or VSCs, the maximum and minimum values will be the desired voltage set points as presented in (39).

$$\begin{aligned}\mathbf{x}_{min}^{\{i\}} = \mathbf{x}_{max}^{\{i\}} &= \mathbf{v_t^{set}}^{\{i\}} \quad \forall i \in \mathcal{I}_{cct} \\ \mathbf{x}_{min}^{\{i\}} = \mathbf{x}_{max}^{\{i\}} &= \mathbf{v_{ac}^{set}}^{\{i\}} \quad \forall i \in \mathcal{I}_{vsc} \\ \mathbf{x}_{min}^{\{i\}} = \mathbf{x}_{max}^{\{i\}} &= \mathbf{v_{dc}^{set}}^{\{i\}} \quad \forall i \in \mathcal{I}_{vscII}\end{aligned} \tag{39}$$

5. Case Study and Simulations

To showcase the effectiveness of the FUBM for the OPF solution of hybrid AC/DC EPS, this section presents a series of test cases and their simulations in AIMMS©. All FUBM simulations have been solved using a PC with CPU Intel Core i7, 2.2GHz and 16GB RAM memory. All cases are solved with diverse solvers as confirmation of the versatility of the model. The first test case will be used to validate the model. The second one will be used as a demonstration of its effectiveness against large scale systems when a series of diverse controls are active. The case also presents the convergence pattern with different solvers. Finally a series of AC and AC/DC test cases are solved and compared to specifically showcase that the FUBM is scalable from small to large systems without sacrificing computational efficiency.

5.1. Validation of the FUBM

The validation of the FUBM is carried out by simulating the test case of Fig. 9. The results are compared against the traditional approach for the calculation of AC/DC grids presented in [43] and [44]. The AC data can be found in [45], and the DC data along with VSC parameters are presented in Table 7.

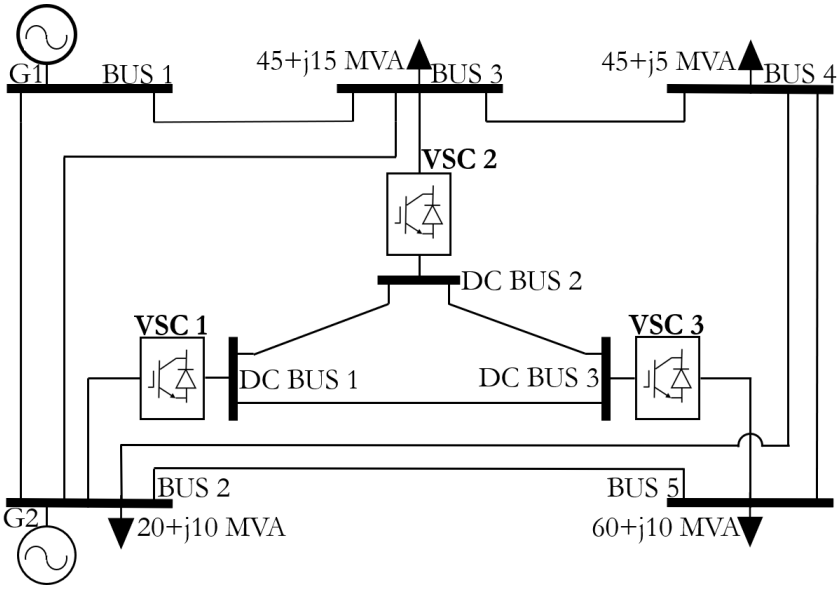

Figure 9: MTDC Stagg Test Case

The objective function of the OPF problem will be the total transmission losses of the test system. They are calculated as shown in (40).

$$f(\mathbf{x}) = \sum_{i=1}^{nl} |P_f^{\{i\}} + P_t^{\{i\}}| \tag{40}$$

TABLE 7
CONVERTERS AND DC GRID PARAMETERS

Parameter	Value
VSC (1,2,3) r_s / x_s	0.0016 p.u. 0.2764 p.u.
VSC Loss Coefficient	$\alpha = \beta = 0, \gamma = 0.01$
DC line r_s (1-2 and 2-3)	0.0260 p.u.
DC line r_s (3-1)	0.0365 p.u.
Max Reactive Power	100 MVAr

The case constraints are specified in Table 8. VSC 1 and 3 are selected as type I and VSC 2 will be regulating the DC voltage magnitude as type II. For all VSC, the optional control variables of θ_{sh} and m_a are optimized.

For the proposed approach, all transmission elements were simulated using the FUBM. The simulation converged in 19 iterations and 0.01 seconds using CONOPT 4.0. Tables 9 and 10 show a comparison of the simulation results between the Traditional and the FUBM approach.

After the comparison of presented in Table 9, it is noticeable that all the voltage magnitudes, phase angles and generators' power outputs were optimized to the same value for both approaches. As expected, for the FUBM, the DC grid has an angle which is different from zero since the voltage angle reference is in the AC grid. Nevertheless, this angle remains constant through the entire DC grid. Thus, the flow of active power in the DC links is solely dictated by the DC nodal voltage magnitude difference (exactly as what it would be in a real DC link). Similarly, the obtained values from the DC grid and VSC power comparison from Table 10 are practically the same. Additionally for the

TABLE 8
MTDC STAGG CONSTRAINTS

Bus ID	Vmin	Vmax	Element	Value [MVA]	
AC 1,2	1	1.02	P_{G1} Min/Max	10	250
AC 3,4,5	0.9	1.1	Q_{G1} Min/Max	-100	100
DC 2	1.01	1.01	P_{G2} Min/Max	-40	40
DC 1,3	0.9	1.1	Q_{G2} Min/Max	-40	40
AC Bus 1	$V_a = 0°$ (Reference)		Element	Value [p.u.]	
Lines Rate	1 MVA (AC & DC)		m_a Min/Max	0.75	1.22

TABLE 9
VOLTAGE AND GENERATION COMPARISON

Bus	Vm [p.u.]		Va [°]	
ID	Traditional	FUBM	Traditional	FUBM
AC 1	1.02	1.02	0	0
AC 2	1.006	1.006	-3.15	-3.15
AC 3	0.992	0.992	-4.92	-4.92
AC 4	0.991	0.991	-5.28	-5.28
AC 5	0.991	0.991	-5.48	-5.48
DC 1	1.015	1.015	***	-26.11
DC 2	1.01	1.01	***	-26.11
DC 3	1.008	1.008	***	-26.11
Generator	Pg [MW]		Qg[MVAr]	
ID	Traditional	FUBM	Traditional	FUBM
G1	129.14	129.14	-8.37	-8.37
G2	40	40	15.04	15.04

TABLE 10
VSC AND DC GRID COMPARISON

	Traditional			FUBM		
	VSC1	VSC2	VSC3	VSC1	VSC2	VSC3
P_f [MW]	-37.58	12.54	24.86	-37.55	12.47	24.86
P_t [MW]	37.9	-12.54	-24.86	37.7	-12.44	-24.79
Q_t [MVAr]	0	-9.07	-6.16	0	-9.04	-6.16
m_a	0.995	1.009	1.003	0.995	1.0087	1.0028
θ_{sh} [°]	***	***	***	-17.0771	-23.1389	-24.5510
B_{eq} [p.u.]	***	***	***	0.03811	0.09360	0.07827
DC Line						
from/to	DC 1-2	DC 2-3	DC 3-1	DC 1-2	DC 2-3	DC 3-1
P_f [MW]	19.17	6.61	-18.24	19.171	6.608	-18.266
P_t [MW]	-19.08	-6.6	18.36	-19.078	-6.597	18.386

FUBM, the values of θ_{sh} and B_{eq} are also obtained. Finally the total losses obtained from each approach are 4.14 MW. The FUBM has been validated.

5.2. Modified Case PEGASE Project

This case accurately represents the size and complexity of part of the European high voltage transmission network. It contains 1,354 buses, 260 generators, 1,991 branches and it operates at 380kV and 220kV. The data stems from the Pan European Grid Advanced Simulation and State Estimation (PEGASE) project [46, 47, 48]. The original case has been modified to incorporate an HVDC Link and a MTDC grid as shown in Fig. 10. Both DC grids operate with a nominal voltage of 345kV and 1000MVA rating. Table 11 summarise the parameters of the DC grids, coupling transformers and VSCs.

The AC node B4231 has been selected to be the voltage angle reference at zero degrees. All the AC and DC transmission elements of the case have been modelled using FUBM. Furthermore, all VSCs type #I have been set for reactive power compensation (*Zero constraint*). Table 12 contains the control settings for all VSCs. Notice even

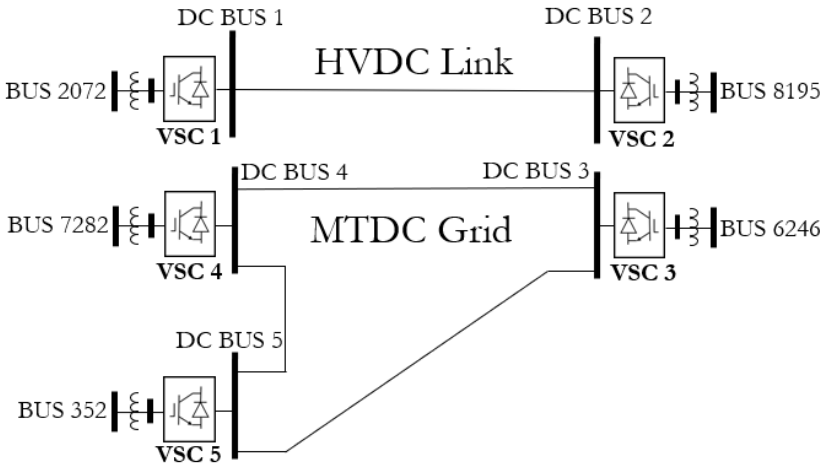

Figure 10: Modified PEGASE Project

TABLE 11
CONVERTER AND DC GRID PARAMETERS

Parameter	Value	
Rating VSC / DC Voltage	1000MVA	345kV
Max / Min DC Voltage	1.1 p.u.	0.9 p.u.
Max / Min m_a	1.22	0.75
Coup. Transformer r_s / x_s	0.0001 p.u.	0.0105 p.u.
VSC (1,2) r_s / x_s	0.0002 p.u.	0.0250 p.u.
VSC (3,4,5) r_s / x_s	0.00015 p.u.	0.00305 p.u.
VSC (1,2) Loss Coefficient	$\alpha = 0.01, \beta = \gamma = 1x10^{-4}$	
VSC (3,4,5) Loss Coefficient	$\alpha = 0.001, \beta = \gamma = 1x10^{-5}$	
DC line r_s (HVDC Link)	0.0005 p.u.	
DC line r_s (MTDC Grid)	0.0007 p.u.	
VSC 2 Droop K_{dp}	5	
VSC 2 Droop P_f^{set}	1 [MW]	
VSC 2 Droop V_f^{set}	1.01 [MW]	
VSC Max Reactive Power	100MVAr	

though all VSCs are operating in one of the explained control modes from Section 3, the control constraints are set individually within the FUBM. Therefore, the model is not restricted to them. As proof of this, the control constraint 2 of the VSC 5 has been left as a free variable. Additionally, two of the existent transformers now are set as a PST and a CTT for power and voltage control respectively. Their settings are also shown in Table 12.

The full Hybrid AC/DC test case optimization problem consist of 44, 728 Constraints and 41, 250 Variables. An average between upper and lower boundaries has been used as initial conditions for all optimization variables. The OPF formulation using FUBM has successfully converged for all solvers, KNITRO 12.0, CONOPT 4.03 and IPOPT 3.11, all of them in AIMMS. Table 13 present the convergence times, iterations and the optimized value of the cost function.

The solver CONOPT preforms the optimization in two steps to find the solution. First it ensures that the infeasibility index is small enough. If the problem is feasible, then it minimizes the objective function while the infeasibility index continues decreasing. On the other hand, the solvers KNITRO and IPOPT reduce infeasibility index while the objective function is minimized. From the results of Table 13, it can be observed that KNITRO and CONOPT are faster solvers in comparison with the IPOPT method. Nevertheless, the final results from the three solvers match for all the variables of the system.

The optimization results for the relevant AC and DC voltages are shown in Table 14. Furthermore, the active and reactive power flows through the control elements and DC lines, as well as their optimized control variables are presented in Table 15. From both tables, it is shown that the results match with the control constraints from Table 12.

TABLE 12
CONTROL SETTINGS FOR VSC AND TRANSFORMERS

Converter	Type	Mode	Const. 1	Const. 2
VSC 1	I	1	Theta = 0	Vac=1.08
VSC 2	III	7	Vdc Droop	Vac=1.075
VSC 3	II	5	Vdc=1.01	Vac=1.06
VSC 4	I	3	Pf=-500	Vac=1.07
VSC 5	I	3	Pf=-450	Vac= free
Transformer	From	To	Control Constraint	
PST	B7466	B3649	Pf = -1.73	
CTT	B6153	B6807	Vt =1.1	

* Power is expressed in MW and Voltage in p.u.

TABLE 13
CONVERGENCE TIME, ITERATIONS AND TOTAL COST

OPF Solver	CONOPT 4.03		KNITRO 12.0	IPOPT 3.11
Infeasibility/Minimization	Infe.	Min.	Infe. & Min.	Infe. & Min.
Iterations	116	27	56	134
Time [s]	19.01	7.23	25.69	271.36
Total Time [s]	26.24		25.69	271.36
Total Gen. Cost [$]	74038.3781		74038.3781	74038.3781

TABLE 14
AC AND DC VOLTAGES

Bus ID	Vm [pu]	Bus ID	Vm [pu]
VSC DC B1	1.00002	VSC AC B2072	1.08000
VSC DC B2	1.00000	VSC AC B8195	1.07500
VSC DC B3	1.01000	VSC AC B6246	1.06000
VSC DC B4	1.01334	VSC AC B7282	1.07000
VSC DC B5	1.01322	CCT AC B6807	1.10000

Additionally, all VSC have satisfactory meet the Zero Constraint for reactive power compensation. Furthermore, the optimal value of B_{eq} has been obtained. Finally, the variable θ_{sh} has been optimized for all active power controlled elements. It is clearly noticeable that a full power control has resulted in both grids.

TABLE 15
OPTIMIZED VARIABLES AND POWER CONTROL

Element ID	Pf [MW]	Theta [deg]	Beq [pu]	ma [tap]
VSC 1	-4.00007	0	-0.17288657	1.07337
VSC 2	3.99999	0	0.02220943	1.07585
VSC 3	946.92069	-52.0451219	0.49999995	1.00112
VSC 4	-500	-33.3258129	0.49999943	1.05951
VSC 5	-450	-36.465037	0.49999931	1.01408
PST	-173	-0.09532315	***	***
CTT	7.28653	***	***	1.04626
DC Line 1-2	4.00007	***	***	***
DC Line 3-4	-481.75773	***	***	***
DC Line 4-5	16.64963	***	***	***
DC Line 5-3	466.64775	***	***	***

Figure 11 presents the minimization of the Cost for the three solvers. Notice that even though all of them are initialized in the same point, the start point varies. This is because the solver KNITRO runs a presolve before starting the optimization. Similarly, CONOPT first solves for the infeasibility and then uses that final state as a starting point

for the minimization. Although the KNITRO solver selected a starting point quite far from the solution, the method is so effective that it manages to converge even before IPOPT and even CONOPT. It is worth to highlight that even though it looks like CONOPT is the fastest, the iterations for the solution of the infeasibility have to be considered, as it was shown in Table 13.

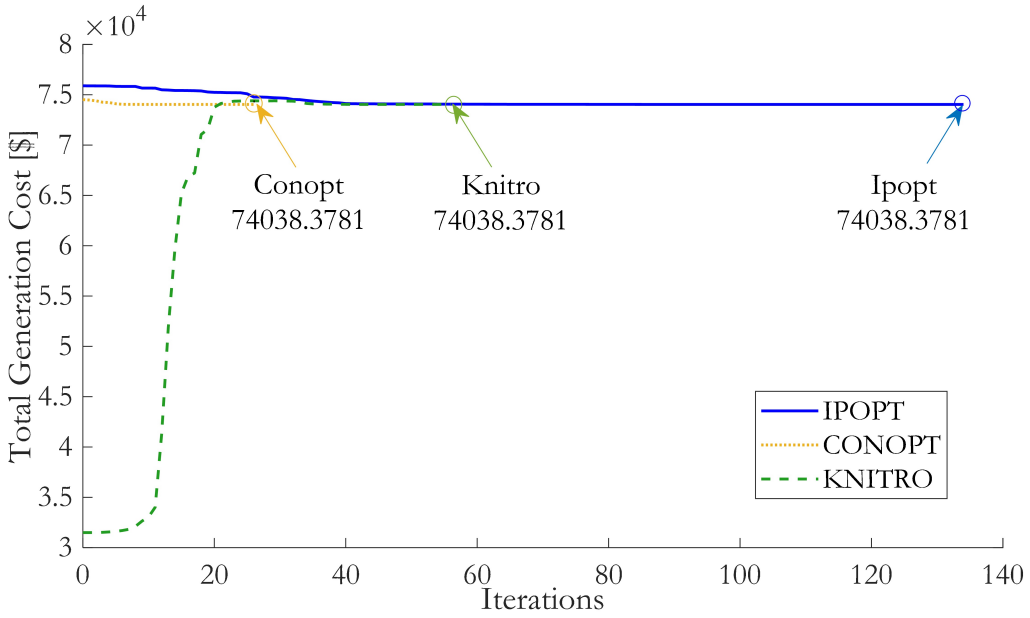

Figure 11: Convergence and Optimal Cost minimization

Figure 12 shows the infeasibility value during the optimization. For the IPOPT solver, the Primal infeasibility, indicates the maximum non-linear constraint violation, and the Dual infeasibility, is measured as the maximum deviation from complementary condition. The start infeasibility index for KNITRO and IPOPT (Primal) was quite high in comparison with CONOPT. Nevertheless it can be seen that their values are dramatically reduced by iteration 20 and 40 respectively. In this graph, again KNITRO has been the fastest solver.

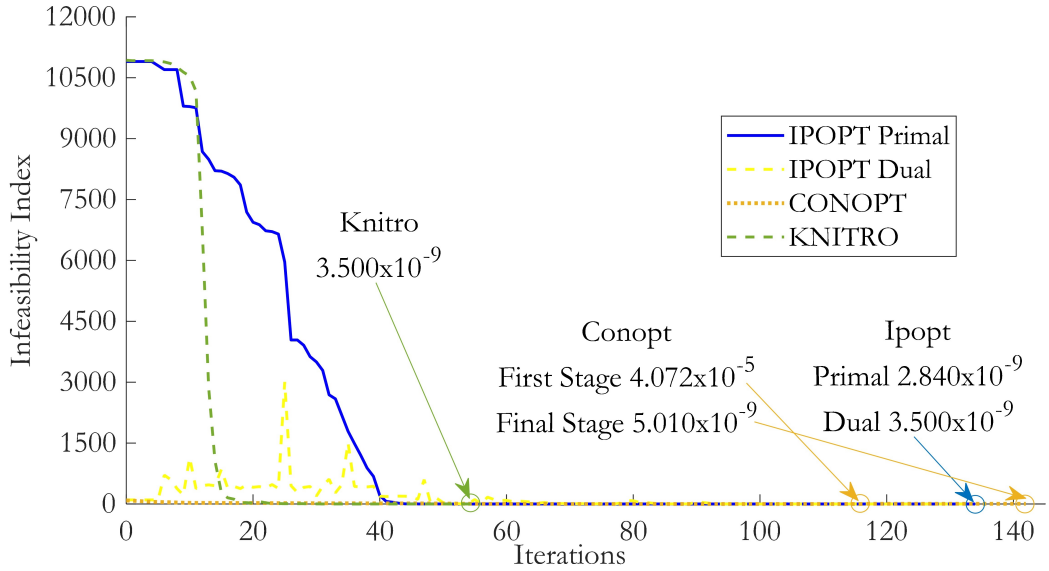

Figure 12: Infeasibility during OPF iterations

5.3. AC and AC/DC Cases for Scalability and Comparison

In this subsection, AC and AC/DC OPF studies are presented to further showcase the capabilities and versatility of applications of the FUBM. AC cases serve as confirmation that the FUBM optional variables do not create any extra computational effort for the AC OPF solution. The results are compared against the open-source tool for electric power system simulation and optimization MATPOWER [20]. AC/DC cases compare the FUBM OPF results with the results obtained in [27], where a Bus Incidence Model (BIM) for ACDC OPF is implemented as an extension of the 'PowerModels.jl' package [49], which is built on top of Julia/JuMP [50]. Both AC and AC/DC cases showcase the scalability and computational performance of the FUBM formulation.

5.3.1. AC test Cases

For the AC OPF scalability and comparison, the IEEE 57 bus test case, and both the 89 and 1354 bus PEGASE cases are solved using the FUBM approach in AIMMS and compared against the results from MATPOWER (V7.0). All the data from the cases are taken from MATPOWER's library. The software and cases data are available in [51].

Table 16 presents the AC OPF results of MATPOWER and AIMMS-FUBM. In order to make a fair comparison, the cases are solved using KNITRO and IPOPT for both MATPOWER and AIMMS-FUBM. Additionally, CONOPT is also used for the FUBM formulation.

TABLE 16
AC OPTIMAL POWER FLOW RESULTS COMPARISON

	MATPOWER				AIMMS-FUBM					
AC	KNITRO		IPOPT		CONOPT 4.03		KNITRO 12.0		IPOPT 3.11	
Cases	Total Cost [$/h]	Time [s]	Total Cost [$/h]	Time [s]	Total Cost [$/h]	Time [s]	Total Cost [$/h]	Time [s]	Total Cost [$/h]	Time [s]
Case 57	41737.77	0.87	41737.79	0.36	41737.79	0.05	41737.79	0.03	41737.79	0.09
Case 89	5819.81	0.39	5819.81	1.12	5814.86	0.19	5814.86	0.16	5814.86	0.41
Case 1354	74069.35	2.51	74069.35	2.96	74069.35	3.56	74069.35	4.28	74069.35	3.5

From Table 16 it is observed that for all test cases the results match, and the computational time is approximately the same. While for the small and medium test cases the AIMMS-FUBM formulation is faster, in the large scale system there is a maximum time difference of 1.77[s] in the solution time. This is to be expected since the solution time in AIMMS includes the creation of the Jacobian and Hessian Matrices of partial derivatives, while for the MATPOWER approach, the derivatives and their structure is predefined in the formulation. Nevertheless the time difference is too small to be considered.

5.3.2. AC/DC Test Cases

A small, a medium, and a large scale AC/DC test system are used to illustrate the scalability and performance of the FUBM formulation. Case-5-ACDC is a modified version of the IEEE 5 bus test system where a three node dc grid has been integrated using VSCs, the data can be found in [52]. Case 24-3 Zones is based on the two area IEEE 24 bus reliability test system which is extended to include a third asynchronous zone. The three areas are connected with two VSC MTDC grids with 3 and 4 DC nodes each one, data is reported in [21]. Finally the AC/DC 3120 bus case represents the Polish system with an interconnected 5 node MTDC grid. This modified large scale system has a total of 3125 buses, 3703 lines and 505 generators, full AC data can be found in [51] and the DC data in [53]. Table 17 presents a comparison of the simulation results reported in [27] for the BIM-JuMP approach, and the AIMMS-FUBM approach. For the FUBM, the AC/DC cases are solved using KNITRO, CONOPT and IPOPT in AIMMS.

It is noticed from Table 17, that the solution from the AIMMS-FUBM formulation has been able to solve and converge to the same results from BIM-JuMP for the three cases. Regarding to the convergence time, it is clearly seen that the AIMMS-FUBM using the CONOPT solver has been the fastest for small, medium and large scale systems. For the large scale system (i.e. Case 3120sp), FUBM-CONOPT is 72.69[s] faster than BIM-IPOPT. The computational times between FUBM-KNITRO and BIM-IPOPT are objectively similar for the three cases, with FUBM-KNITRO slightly outperforming BIM-IPOPT for the largest scale system. The results for the small and medium cases using FUBM-IPOPT are also objectively similar to BIM-IPOPT. On the other hand, for the 3120 case, even though AIMMS-FUBM converged to a slightly better total cost, the BIM-IPOPT was faster, however it is worth noting that in both instances the convergence time is within the same order of magnitude.

TABLE 17
AC/DC OPTIMAL POWER FLOW RESULTS COMPARISON

	BIM-JuMP		AIMMS-FUBM								
AC/DC	IPOPT		CONOPT 4.03			KNITRO 12.0			IPOPT 3.11		
Cases	Total Cost [$/h]	Time [s]	Total Cost [$/h]	Time [s]	Iter.	Total Cost [$/h]	Time [s]	Iter.	Total Cost [$/h]	Time [s]	Iter.
Case5	194.14	0.20	194.14	0.07	17	194.14	0.08	43	194.14	0.17	46
Case24-3z	150228.00	0.17	150227.09	0.14	42	150227.09	0.18	25	150227.09	0.23	26
Case 3120sp	2142635.0	122.7	2142635.0	50.01	157	2142635.0	118.23	60	2142634.9	298.7	479

6. Conclusion

In this paper, a steady-state FUBM model for the OPF solution of hybrid AC/DC EPS has been presented. The proposed FUBM model is capable of seamlessly modelling a variety of network elements, both AC and DC, including PSTs, CTTs, and more importantly VSC and VSC-interfaced elements including point-to-point and multi-terminal HVDC links used to create hybrid AC/DC networks. All model elements are represented using a common model representation with shared variables and parameters that depending on the model type may or may not be activated. Meanwhile, when modelling AC/DC grids, there is no need for introducing additional coupling constraints to maintain power balance between AC and DC parts of the network as FUBM model structure is configured in such a way that from a purely mathematical perspective, there is no distinction between AC and DC counterparts. Thus, same AC power flow equations can be used to solve the entire hybrid EPS capturing any interactions between interconnected grids. Control elements are represented explicitly by their associated control variables and constraints on voltage and power flows when needed depending on the network operational requirements. Meanwhile, realistic operational limits may be enforced through the *in-model* structures simply by extending the constraints set in the OPF formulation pertaining to any control elements. Moreover, when modelling VSCs using the FUBM, switching losses are calculated using a quadratic correction just as stated in [32]. Thanks to its ability of simulating all the aforementioned *in-models* there is no need to analyse the system equations model by model thereby from a software perspective reducing the need for developing separate model libraries for several network elements. A comparison against the Traditional approach for Validation of the model has been presented. Furthermore, simulation results over the modified large scale Pegase system demonstrate full power and voltage control over several elements of the hybrid AC/DC grid whilst maintaining a good degree of convergence and accuracy of the solution. Finally, the FUBM has been successfully tested for small, medium and large-scale AC and AC/DC systems, where the FUBM has proved to be working with a variety of optimization solvers without sacrificing any computational effort, even presenting faster results in some cases. Simulation results indicate that the FUBM model is flexible enough to be solved with a variety of solvers using general purpose model-based languages such as AIMMS. Considering that (i) All the components of the FUBM are either the same or an equivalent component for the Traditional models, and (ii) The FUBM formulation solves OPF hybrid transmission AC/DC grids using traditional AC OPF equations, then, any convexification, linear approximation or robust optimization applied to the AC OPF could be also applied as future research of the FUBM approach. The versatility and prowess of the FUBM plus its adaptability in modelling a variety of network elements both AC and DC makes it a suitable candidate and a formidable tool at the hands of the TSOs and network analysts for large-scale steady-state EPS studies without sacrificing computational efficiency and accuracy of the solution.

References

[1] U. Nations, "Report of the Conference of the Parties on its 21st session," *Framework Convention on Climate Change, Conference of the Parties*, Dec. 2015.

[2] N. Grid, "Future energy scenareos, system operator," *National Grid Reports*, Jul. 2018.

[3] M. E. Economics, "EEnergy informer, the international energy newsletter," *EEnergy Informer*, Jan. 2019.

[4] ENTSO-e. (2020) Ten-year network development plan (tyndp) 2020. [Online]. Available: https://tyndp.entsoe.eu/documents/

[5] R. T. Pinto, A. C. Leon-Ramirez, M. Aragues-Penalba, A. Sumper, and E. Sorrentino, "A fast methodology for solving power flows in hybrid AC/DC networks: The european north sea supergrid case study," in *PCIM Europe 2016*, Nuremberg, Germany, May 2016.

[6] ENTSO-e. (2019, May) Value of timely implementation of "better projects". [Online]. Available: https://www.entsoe.eu/2019/05/20/value-of-timely-implementation-of-better-projects/

[7] ——. (2018, Dec.) Improving hvdc system reliability. [Online]. Available: https://www.entsoe.eu/2018/12/10/improving-hvdc-system-reliability/

[8] E. Bompard, G. Fulli, M. Ardelean, and M. Masera, "It's a bird it's a plane it's a...Supergrid!: Evolution opportunities and critical issues for Pan-European transmission," *IEEE Power and Energy Magazine*, vol. 12, no. 2, pp. 40–50, Feb. 2014.

[9] ENTSO-e. (2019, Apr.) R and i roadmap 2017–2026. [Online]. Available: https://www.entsoe.eu/publications/research-and-development/

[10] R. Irnawan, *Planning and Control of Expandable Multi-Terminal VSC-HVDC Transmission Systems*, 1st ed. Aalborg University, Aalborg Denmark: Springer Nature, 2019.

[11] ENTSO-e. (2020, Feb.) Operational limits and conditions for frequency coupling. [Online]. Available: https://www.entsoe.eu/publications/system-operations-reports/

[12] E. Acha, P. Roncero-Sánchez, A. de la Villa-Jaen, L. M. Castro, and B. Kazemtabrizi, *VSC-FACTS-HVDC: Analysis, Modelling and Simulation in Power Grids*. Laboratory of Electrical Energy Engineering, Tampere University of Technology, Finland: Wiley, 2019.

[13] A. Wood, B. Wollenberg, and G. Sheblé, *Power generation operation and control*, 3rd ed. New Jersey, USA: Wiley-IEEE Press, 2014.

[14] Y. Wen, J. Zhan, C. Chung, and W. Li, "Frequency stability enhancement of integrated AC/VSC-MTDC systems with massive infeed of offshore wind generation," *IEEE Transactions on Power Systems*, pp. 1–10, Jan. 2018.

[15] W. Feng, A. L. Tuan, L. B. Tjernberg, A. Mannikoff, and A. Bergman, "A new approach for benefit evaluation of multiterminal VSC–HVDC using a proposed mixed AC/DC optimal power flow," *IEEE Transactions on Power Delivery*, pp. 432–443, Jul. 2013.

[16] Z. di Wang, K.-J. Li, J. guo Ren, L.-J. Sun, J.-G. Zhao, Y.-L. Liang, W.-J. Lee, and Z. hao Ding, "A coordination control strategy of voltage-source-converter-based MTDC for offshore wind farms," *IEEE Transactions on Industry Applications*, pp. 2743–2752, Feb. 2015.

[17] J. Beerten and R. Belmans, "A comprehensive modeling framework for dynamic and steady state analysis of voltage droop control strategies in HVDC grids," *International Journal of Electrical Power and Energy Systems*, vol. 73, Dec. 2015.

[18] Z. Yang, H. Zhong, A. Bose, Q. Xia, and C. Kang, "Optimal power flow in ACDC grids with discrete control devices," *IEEE Transactions Power Systems*, vol. 33, Mar. 2018.

[19] B. Stott, O. Alsac, and A. Monticelli, "Security analysis and optimization," *IEEE Transactions on Power Systems*, vol. 12, no. 1, p. 1623–1644, Feb. 1987.

[20] R. D. Zimmerman, C. E. Murillo-Sánchez, , and R. J. Thomas, "MATPOWER: Steady-state operations, planning and analysis tools for power systems research and education," *Power Systems, IEEE Transactions on*, vol. 26, no. 1, pp. 12–19, Feb. 2011.

[21] J. Beerten and R. Belmans, "Development of an open source power flow software for high voltage direct current grids and hybrid ACDC systems MATACDC," *IET Generation Transmission Distribution*, vol. 9, no. 10, pp. 966 – 974, Jun. 2015.

[22] SIEMENS, *PSS®E Transmission Planning and Operations Software for the Power Industry*. Freyeslebenstrasse 1 91058 Erlangen, Germany: SIEMENS Energy Management Division, 2019.

[23] DIgSILENT, *Power Factory-Power system analysis software*. Heinrich-Hertz-Straße 9 72810 Gomaringen, Germany: DIgSILENT, 2019.

[24] T. LEVERINGHAUS, T. BREITHAUPT, S. GARSKE, and L. HOFMANN, "Modelling of sequential optimal power flow by piecewise linear convexificated quadratic approximations," in *2018 International Conference on Power System Technology (POWERCON)*, 2018, pp. 87–92.

[25] W. Wei, J. Wang, N. Li, and S. Mei, "Optimal power flow of radial networks and its variations: A sequential convex optimization approach," *IEEE Transactions on Smart Grid*, vol. 8, no. 6, pp. 2974–2987, 2017.

[26] I. M. Nejdawi, K. A. Clements, and P. W. Davis, "An efficient interior point method for sequential quadratic programming based optimal power flow," *IEEE Transactions on Power Systems*, vol. 15, no. 4, pp. 1179–1183, 2000.

[27] H. Ergun, J. Dave, D. Van Hertem, and F. Geth, "Optimal power flow for ac–dc grids: Formulation, convex relaxation, linear approximation, and implementation," *IEEE Transactions on Power Systems*, vol. 34, no. 4, pp. 2980–2990, 2019.

[28] M. Hotz and W. Utschick, "hynet: An optimal power flow framework for hybrid ac/dc power systems," *IEEE Transactions on Power Systems*, vol. 35, no. 2, pp. 1036–1047, 2020.

[29] A. Alvarez-Bustos and B. Kazemtabrizi, "Flexible general branch model unified power flow algorithm for future flexible AC/DC networks," in *2018 IEEE International Conference on Environment and Electrical Engineering (EEEIC / I&CPS Europe)*, Palermo, Italy, Jun. 2018.

[30] E. Acha, B. Kazemtabrizi, and L. M. Castro, "A new VSC-HVDC model for power flows using the Newton-Raphson method," *IEEE Transactions on Power Systems*, vol. 28, no. 3, pp. 2602–2612, Aug. 2013.

[31] R. Chai, B. Zhang, J. Dou, Z. Hao, and T. Zheng, "Unified power flow algorithm based on the NR method for hybrid AC/DC grids incorporating VSCs," *IEEE Transactions on Power Systems*, vol. 31, no. 6, pp. 4310 – 4318, Nov. 2016.

[32] I. E. C. (IEC), "IEC 62751-2 Power losses in voltage sourced converter (VSC) valves for high-voltage direct current (HVDC) systems - Part 2 Modular multilevel converters," *IEC International Standard*, Aug. 2014.

[33] S. Johansson, G. Asplund, E. Jansson, and R. Rudervall, "Power system stability benefits with VSC DC-transmission systems," in *in Proc. CIGRE 2004 Session*, Paris, France, 2004.

[34] W. Feng, L. A. Tuan, L. B. Tjernberg, A. Mannikoff, and A. Bergman, "A new approach for benefit evaluation of multiterminal vsc–hvdc using a proposed mixed ac/dc optimal power flow," *IEEE Transactions on Power Delivery*, vol. 29, no. 1, pp. 432–443, 2014.

[35] B. Kazemtabrizi and E. Acha, "An advanced STATCOM model for optimal power flows using Newton's method," *IEEE Transactions on Power Systems*, vol. 29, Mar. 2014.

[36] L. Gyugyi, C. D. Schauder, S. L. Williams, T. R. Rietman, D. R. Torgerson, and A. Edris, "The unified power flow controller: a new approach to power transmission control," *IEEE Transactions on Power Delivery*, vol. 10, no. 2, pp. 1085–1097, 1995.

[37] L. Liu, P. Zhu, Y. Kang, and J. Chen, "Power-flow control performance analysis of a unified power-flow controller in a novel control scheme," *IEEE Transactions on Power Delivery*, vol. 22, no. 3, pp. 1613–1619, 2007.

[38] D. Jovcic, "Bidirectional, high-power dc transformer," *IEEE Transactions on Power Delivery*, vol. 24, no. 4, pp. 2276–2283, 2009.

[39] J. Beerten, S. Cole, and R. Belmans, "Generalized steady-state VSC MTDC model for sequential AC/DC power flow algorithms," *IEEE Transactions on Power Systems*, vol. 27, no. 2, pp. 821–829, May 2012.

[40] T. K. Vranaa, J. Beertenb, R. Belmans, and O. B. Fosso, "A classification of DC node voltage control methods for HVDC grids," *Electric Power Systems Research*, pp. 137–144, Oct. 2013.

[41] W. Wang and M. Barnes, "Power flow algorithms for multi-terminal vsc-hvdc with droop control," *IEEE Transactions on Power Systems*,

vol. 29, no. 4, pp. 1721–1730, 2014.
[42] Z. Li, J. He, Y. Xu, and X. Wang, "An optimal power flow algorithm for AC/DC hybrid power systems with VSC-Based MTDC considering converter power losses and voltage-droop control strategy," *IEEJ Transactions on electrical and electronic engineering*, Jun. 2018.
[43] JavierRenedo, A. A. Ibrahim, B. Kazemtabrizi, A. García-Cerrada, L. Rouco, Q. Zhao, and J. García-González, "A simplified algorithm to solve optimal power flows in hybrid VSC-based ACDC systems," *International Journal of Electrical Power and Energy Systems - El Sevier*, vol. 110, 2019.
[44] Q. Zhao, J. Garcia-Gonzalez, O. Gomis-Bellmunt, E. Prieto-Araujo, and F. M. Echavarren, "Impact of converter losses on the optimal power flow solution of hybrid networks based on VSC-MTDC," *Electric Power Systems Research*, vol. 151, p. 395–403, 2017.
[45] G. W. Stagg and A. H. El-Abiad, *Computer Methods in Power System Analysis*, 9th ed. New York: McGraw-Hill, 1971.
[46] S. Fliscounakis, P. Panciatici, F. Capitanescu, and L. Wehenkel, "Contingency ranking with respect to overloads in very large power systems taking into account uncertainty, preventive and corrective actions," *IEEE Transactions Power Systems*, vol. 28, Nov. 2013.
[47] C. Josz, S. Fliscounakis, J. Maeght, and P. Panciatici. (2013) Ac power flow data in matpower and qcqp format: itesla, rte snapshots, and pegase. [Online]. Available: https://arxiv.org/abs/1603.01533
[48] ENTSO-e. (2014) Common information model (cim) for grid models exchange. [Online]. Available: https://www.entsoe.eu/digital/common-information-model/cim-for-grid-models-exchange/#cgmes-conformity
[49] C. Coffrin, R. Bent, K. Sundar, Y. Ng, and M. Lubin, "Powermodels.jl: An open-source framework for exploring power flow formulations," *in Proc. Power Syst. Comput. Conf.*, vol. 20, 2018.
[50] I. Dunning, J. Huchette, , and M. Lubin, "Jump: A modeling language for mathematical optimization," *SIAM Rev.*, vol. 59, no. 2, p. 295–320, 2017.
[51] R. D. Zimmerman and C. E. Murillo-Sanchez. (2020) Matpower software version 7.0. [Online]. Available: https://matpower.org
[52] J. Beerten, D. Van Hertem, and R. Belmans, "Vsc mtdc systems with a distributed dc voltage control - a power flow approach," in *2011 IEEE Trondheim PowerTech*, 2011, pp. 1–6.
[53] J. Rimez and R. Belmans, "A combined ac/dc optimal power flow algorithm for meshed ac and dc networks linked by vsc converters," *Int. Trans. Elect. Energy Syst*, vol. 25, no. 10, p. 2024–2035, 2015.

Abraham Alvarez-Bustos was born in Mexico. He received a B.Sc. degree in Electrical Engineering from Instituto Politecnico Nacional (IPN) - ESIME, Mexico City, Mexico, in 2012. Then, a M.Sc. degree in Electrical Power Systems from the IPN - Sección de Estudios de Posgrado e Investigación (SEPI), Mexico City, Mexico, in 2015, where he got First Class Honours and an Honorific Mention. In 2016 he worked as a Transmission System Analyst in the National Control Centre of Energy (CENACE), Mexico. He is currently pursuing the Ph.D. degree at Durham University, Durham, UK in the area of Power Systems optimization and Control. He is a fully Funded PhD Student by Consejo Nacional de Ciencia y Tecnología (CONACyT) and Secretaría de Energía (SENER), México.

Dr Behzad Kazemtabrizi is Assistant Professor in Electrical Engineering in the department of engineering at Durham University. He has obtained his PhD in Electrical Engineering – Power Systems from Glasgow University in 2011. His principal research interests are in advanced power systems modelling, for improving operability and reliability of future flexible power systems. His past and present research encompasses a wide area of topics including but not limited to research in energy systems integration, reliability and optimization of power systems, and large-scale wind energy integration.

Dr Mahmoud Shahbazi is an Assistant Professor in the Department of Engineering and Early Career Fellow in the Durham Energy Institute (DEI) at Durham University, UK. His research is mainly focused on Power Electronics, Renewable Energy Integration, Electric Drives, Microgrid, Smart Grid, Power Electronic Converters, Monitoring, Fault-Tolerant Control Operation, Electrical and Thermal Storage optimization in Virtual Power Plants as well as Modelling and optimization of AC/DC Power Grids.

Prof Enrique Acha-Daza was born in Mexico. He graduated from Universidad Michoacana in 1979 and received the Ph.D. degree from the University of Canterbury, Christchurch, New Zealand, in 1988. He was a Professor of Electrical Power Systems at the University of Glasgow, Glasgow, U.K., in 2001–2011 and he is now a Professor of Electrical Power Systems at the Tampere University of Applied Sciences (TAMK), Tampere, Finland. Prof. Acha is an IEEE PES Distinguished Lecturer.